Theor Chem Acc (2009) 124:225–234
DOI 10.1007/s00214-009-0603-3

REGULAR ARTICLE

Theoretical investigation of chemosensor for fluoride anion based on amidophthalimide derivatives

Ruifa Jin · Jingping Zhang

Received: 19 January 2009 / Accepted: 25 June 2009 / Published online: 5 July 2009
© Springer-Verlag 2009

Abstract The interactions among chemosensor substrate, 4-benzoylamido-*N*-methylphthalimide (BMP1), and different halide anions (F^-, Cl^-, and Br^-) have been theoretically investigated at the B3LYP/6-31+G(d) level with the basis set superposition error correction. It turned out that the intermolecular proton transfer causes the colorimetric and fluorescent signaling of BMP1 for F^-. The deprotonated complex $BMP1^-\cdots H^+\cdots F^-$ is formed for the deprotonation process of chemosensor, and the P orbitals of F^- play the key role in the prediction of the optical properties of $BMP1^-\cdots H^+\cdots F^-$. The inclusion of diffuse functions to the basis set has a significant effect in the structural optimization for investigated complexes. The properties of six designed BMP1 derivatives [containing –CN and/or $-N(CH_3)_2$ substituent(s)] have been calculated. Our results suggest that the mono-substituted (on the methylphthalimide moiety) and bi-substituted [$-N(CH_3)_2$ and –CN groups on benzoylamido and methylphthalimide moieties, respectively] derivatives are expected to be the promising candidates for ratiometric fluorescent fluoride chemosensors as well as chromogenic chemosensor, whereas for mono-substituted (on the benzoylamido moiety) and bi-substituted [–CN and $-N(CH_3)_2$ on benzoylamido and methylphthalimide moieties, respectively] derivatives can serve as chromogenic fluoride chemosensor only. Furthermore, the derivatives with mono-CN substituents are promising luminescent materials for organic light emitting diodes as well.

Keywords Chemosensor · Basis set superposition error (counterpoise) correction · Intramolecular charge transfer (ICT) · UV–Vis and fluorescence spectra · Halide anions · Amidophthalimide

1 Introduction

The development of fluorescent chemosensors for anions has drawn much attention in recent years, because anions play important roles in clinical biochemistry and environment [1–8]. Sensors based on anion-induced fluorescence change appear to particularly be attractive due to its simplicity and high sensitivity [9–14]. For quantitative analyses, ratiometric chemosensors have significant advantages of their dual emission system, which can minimize the measurement errors caused by fluctuations of light scattering as well as reagent concentration [15]. The smallest anion, F^-, has unique chemical properties. It is of particular interest to detect it owing its essential roles in a broad range of biological, medical, and chemical processes of osteoporosis, fluorination of drinking water supplies, or even in chemical and nuclear warfare agents [16–22]. Different signaling mechanisms have been suggested for fluoride chemosensor, such as photoinduced electron transfer [23–26], excited state proton transfer [27–30], intramolecular charge transfer (ICT) [31–33], excimer and exciplex formation [34–36], and metal–ligand charge transfer [37, 38], and so on.

Recently, a ratiometric fluorescent fluoride chemosensor as well as chromogenic chemosensor made of

Electronic supplementary material The online version of this article (doi:10.1007/s00214-009-0603-3) contains supplementary material, which is available to authorized users.

R. Jin · J. Zhang (✉)
Faculty of Chemistry, Northeast Normal University, Changchun 130024, China
e-mail: zhangjingping66@yahoo.com.cn

R. Jin
Department of Chemistry, Chifeng College, Chifeng 024000, China

Scheme 1 Geometries of the model compound BMP1 and its derivatives BMP*n* ($n = 2$–7) and their deprotonation chemosensing for F^-, along with atom numbering

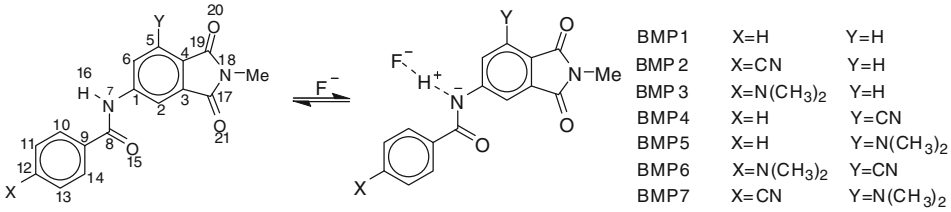

4-benzoylamido-*N*-methylphthalimide (BMP1, Scheme 1) has been reported [39]. F^--induced color change allows its detection with naked eyes. The changes of the electronic absorption and fluorescence behavior of BMP1 are due to F^--induced deprotonation of the 4-amido moiety. Geometries of the halide complexes BMP1·X (X = F^- and Cl^-) have been optimized in the ground state (S_0) at the B3LYP/STO-3G level without considering basis set superposition error (BSSE) correction [40, 41]. Recently, the efficiency and electro-optical properties of *N*-(2-methyl-1,3-dioxo-indan-5-yl)-benzamide and its derivatives have been investigated [42]. However, to our knowledge, neither calculations about the first excited singlet state (S_1), the electronic absorption, and fluorescence behaviors of BMP1 and its halide complexes BMP1·X or anion form ($BMP1^-$) nor sophisticated level optimization for S_0 with BSSE corrections have been reported so far.

Herein we report the investigation of both host–guest interaction and signaling properties from theoretical point of view for this system. Further in-depth explanations for the experimental results have been discussed by the investigation of the optical and electronic properties of BMP1. To investigate the substituent effect, several derivatives (BMP*n*, $n = 2$–7) with electron-donating [–$N(CH_3)_2$] and/or electron-withdrawing (–CN) groups, as shown in Scheme 1, have been designed to provide a demonstration for the rational design of new fluorescent and/or chromogenic chemosensors for fluoride anion, as well as some candidates for organic light emitting diodes (OLEDs) material [43–52].

2 Computational details

Six BMP1 derivatives by introducing electron-donating [–$N(CH_3)_2$] or -withdrawing (–CN) group on either X and/or Y position or both (BMP*n*, $n = 2$–7, Scheme 1) have been designed.

All calculations have been performed using Gaussian 03 code [53]. Optimizations have been carried out without symmetry constraints. The geometry optimizations of neutral forms BMP*n* for S_0 have been obtained at the B3LYP [54] level using both 6-31G(d) and 6-31+G(d) basis sets. Single diffuse function has been added to the 6-31G(d) basis set to evaluate the basis set effect. Halide complexes $BMPn^-\cdots H^+\cdots F^-$, BMP*n*·$Cl^-$, and BMP*n*·$Br^-$ ($n = 1$–7) have been optimized at the same theoretical levels as above with the consideration of BSSE correction using the counterpoise method [40, 41]. The S_1 structures for neutral forms BMP*n* and deprotonated complexes $BMPn^-\cdots H^+\cdots F^-$ (Scheme 1) have been optimized at the CIS [55] level using the 6-31+G(d) basis set. The harmonic vibrational frequency calculations using the same methods as for the geometry optimizations were used to ascertain the presence of a local minimum. Absorption and fluorescent properties of BMP*n* and $BMPn^-\cdots H^+\cdots F^-$ ($n = 1$–7) have been predicted using the TD-DFT/6-31+G(d) method based on the S_0 and S_1 optimized geometries, respectively, which has been proved to be efficient in providing proper optical properties [32, 56, 57]. The MeCN solvent effect has also been considered using the Polarized Continuum Model (PCM) [58].

The geometry optimizations for the S_1 of BMP1 and $BMP1^-\cdots H^+\cdots F^-$ were also carried out at the TD-B3LYP/6-31+G(d,p) level by TURBOMOLE 5.7 [59] program suite. As the geometry optimization of $BMP1^-\cdots H^+\cdots F^-$ was failed to be converged, only the fluorescent property of BMP1 was predicted (411.42 nm), which was similar to that using the same method based on the optimized geometry at the CIS/6-31+G(d) level (in MeCN solvent, see Table 2). Furthermore, the predicted fluorescent property of both BMP1 and $BMP1^-\cdots H^+\cdots F^-$ based on the optimized geometry at the CIS/6-31+G(d) level are in good agreement with experimental result (see Table 2). Hence, the S_1 structures for neutral forms BMP*n* and their halide complexes $BMPn^-\cdots H^+\cdots F^-$ and BMP1·X (X = Cl^- and Br^-, $n = 1$–7) have been optimized at the CIS/6-31+G(d) level.

To predict the stability of the BMP1 and its substituted derivatives BMP*n* ($n = 2$–7) from a viewpoint of molecular orbital theory, the absolute hardness, η, and the absolute electronegativity, χ, of the BMP*n* ($n = 1$–7) were calculated using operational definitions [60–63] given by Eqs. 1 and 2, respectively.

$$\eta = \frac{1}{2}\left(\frac{\partial \mu}{\partial N}\right) = \frac{1}{2}\left(\frac{\partial^2 E}{\partial N^2}\right) = \frac{I - A}{2} \tag{1}$$

$$\chi = -\mu = -\left(\frac{\partial E}{\partial N}\right) = \frac{I + A}{2} \tag{2}$$

where μ is the chemical potential and N is the total electron number. In this study, the values for I (ionization potential) and A (electron affinity) are calculated using Koopmans' theorem [64] based on the optimized geometries at the B3LYP/6-31+G(d) level.

The radiative rate constants (k_f) of the BMPn (n = 1–7) and their deprotonated complexes were calculated using Einstein's spontaneous emission transition probability relation [65–67]:

$$k_f = \frac{f v^2}{1.50}$$

where k_f is the radiative rate constant (in s^{-1}), v is the transition wavenumber (in cm^{-1}), and f is the corresponding oscillator strength.

3 Results and discussions

3.1 Host–guest interaction and diffuse function effect on the equilibrium geometry of complexes BMP1$^-$···H$^+$···F$^-$ and BMP1·X (X = Cl$^-$ and Br$^-$)

Using BMP1 as the model compound, the interaction between host and guest has been investigated. Table 1 presents the most important geometrical parameters and interaction energies optimized at the B3LYP/6-31G(d) and B3LYP/6-31+G(d) levels with and without BSSE corrections for complexes BMP1$^-$···H$^+$···F$^-$ and BMP1·X (X = Cl$^-$ and Br$^-$). According to the suggested cutoff definition for D–H···A H-bond (H···A distances <3.0 Å and D–H···A angles >110°) [68, 69], the interaction between amido-H and halide anion has been considered as H-bond, which has been named as incipient (frozen) proton transfer reaction from D to A [69].

Both geometries and interaction energies for complexes are quite basis set dependent, especially for BMP1$^-$···H$^+$···F$^-$, as shown in Table 1. For BMP1$^-$···H$^+$···F$^-$ without BSSE correction, the optimized distances between amido N and H ($R_{N–H}$), the H-bond lengths between H and F$^-$ ($R_{H···F}$), and the dihedral angles $\theta_{C1N7H16F}$ are highly diffuse function dependent. The deviations between 6-31G(d) and 6-31+G(d) basis set are 0.038 and 0.097 Å, and 46°, respectively. The diffuse function dependency is also significant on the equilibrium geometry of BMP1$^-$···H$^+$···F$^-$ even considering BSSE correction, where the deviations between 6-31G(d) and 6-31+G(d) basis set are 0.69 and 0.44 Å, and 64°, respectively. Comparing the optimized geometries of BMP1$^-$···H$^+$···F$^-$ using the 6-31+G(d) and 6-31G(d) basis sets with BSSE correction, one can see that the amido H and fluoride atoms move out of the molecular plane by using 6-31G(d) basis set, while the structure of complex BMP1$^-$···H$^+$···F$^-$ is almost planar by using 6-31+G(d) basis set. Moreover, comparing the optimized geometries using the 6-31+G(d) basis set with and without BSSE correction, the deviations of the $R_{N–H}$, $R_{H···F}$, and the dihedral angle $\theta_{C1N7H16F}$ for BMP1$^-$···H$^+$···F$^-$ are only 0.002 and 0.012 Å, and 0.04°, respectively. Therefore, the BSSE correction dependency is dramatically reduced after the inclusion of diffuse function to 6-31G(d) basis set. Furthermore, the difference between the interaction energies (ΔE) and the BSSE-corrected one (ΔE_{BSSE}) at the B3LYP/6-31G(d) level is about 27 kcal/mol, while the corresponding value at the B3LYP/6-31+G(d) level is only about 2 kcal/mol. This indicates that the deviation between the with and without BSSE-corrected interaction energies is dramatically reduced by the inclusion of diffuse function to 6-31G(d) basis set. In order to assess whether 6-31+G(d) basis set gives converged results or not, we have performed geometry optimizations and interaction energies

Table 1 Distances of $R_{N–H}$ and $R_{H···X}$ (in angstroms), angles of $\theta_{N–H···X}$ (in degree), dihedral angles of $\theta_{C1N7H16F}$ (in degree), and interaction energies with and without BSSE corrections (in kcal/mol) for complexes BMPn^-···H$^+$···F$^-$, BMPn·Cl$^-$, and BMPn·Br$^-$ at the B3LYP/6-31+G(d) level

Species	Without BSSE					With BSSE				
	$R_{H–N}$	$R_{H···X}$	$\theta_{N–H···X}$	$\theta_{C1N7H16X}$	ΔE	$R_{H–N}$	$R_{H···X}$	$\theta_{N–H···X}$	$\theta_{C1N7H16X}$	ΔE_{BSSE}
BMP1	1.011 (1.011)									
BMPn^-···H$^+$···F$^-$	1.109 (1.147)	1.402 (1.305)	171.7 (171.5)	0.07 (46.9)	−57.0 (−101.9)	1.107 (1.793)	1.414 (0.970)	171.7 (173.3)	0.03 (64.5)	−55.2 (−74.5)
BMP1·Cl$^-$	1.036 (1.309)	2.274 (2.227)	167.8 (168.2)	−0.01 (−0.01)	−32.1 (−37.6)	1.036 (1.038)	2.281 (2.255)	167.8 (168.0)	−0.008 (−0.012)	−31.8 (−34.2)
BMP1·Br$^-$	1.033 (1.306)	2.419 (2.415)	167.1 (167.9)	0.06 (0.14)	−35.6 (−39.6)	1.030 (1.035)	2.542 (2.480)	167.1 (167.5)	1.7 (1.5)	−27.7 (−34.5)

Data in parenthesis are obtained at the B3LYP/6-31G(d) level

(ΔE and ΔE_{BSSE}) of $BMP1^-\cdots H^+\cdots F^-$ with and without BSSE corrections at the B3LYP level with a series of basis sets. The results (see Supplementary Tables SI and SII) indicated that 6-31+G(d) basis set gives converged results. Therefore, addition of diffuse function to 6-31G(d) basis set is necessary for the optimization of this kind of system, hereafter, we will discuss the complex structures using the counterpoise method and 6-31+G(d) basis set. Compared with the N–H bond in BMP1 (1.011 Å), obviously, the N–H bond is stretched (>0.096 Å elongation) and H^+ moves close to F^- with $R_{N-H} = 1.107$ Å and $R_{H\cdots F} = 1.414$ Å in $BMP1^-\cdots H^+\cdots F^-$, or more precisely as deprotonated complex $BMP1^-\cdots H^+\cdots F^-$. However, in other halide cases, N–H distance only slightly elongated (<0.03 Å, Table 1). Therefore, the host chemosensor substrate prefers to bind with F^- anion and forms the most stable complex $BMP1^-\cdots H^+\cdots F^-$.

It is clear that the BSSE-corrected interaction energy (ΔE_{BSSE}) of complex $BMP1{\cdot}F^-$ is much more favorable for the distinct selectivity of F^- anion than other halides, as shown in Table 1. At the B3LYP/6-31+G(d) level, the ΔE_{BSSE} of $BMP1^-\cdots H^+\cdots F^-$ is more than those of $BMP1{\cdot}Cl^-$ and $BMP1{\cdot}Br^-$ by about 23 and 27 kcal/mol, respectively. Therefore, the sensor can easily detect F^- in the presence of Cl^- and Br^-. These calculation results are in good agreement with the reported experimental observations that intermolecular proton transfer between chemosensor substrate of BMP1 and F^- anion occurs when the concentration of F^- anions reaches certain level from the addition of tetrabutylammonium fluoride to the sensor substrate solution [39].

3.2 Spectral simulation

On the basis of the B3LYP/6-31+G(d) and CIS/6-31+G(d) optimized geometries for the S_0 and S_1, respectively, the absorption and fluorescence spectra have been predicted using various functionals such as TD-B3LYP, TD-PBE0, TD-BLYP, TD-OLYP, TD-BHandH, TD-BHandHLYP, TD-MPWB95, TD-MPWLYP, and TD-SVWN with 6-31+G(d) basis set. Table 2 presents the λ_{abs} and λ_{fl} of BMP1 and $BMP1^-\cdots H^+\cdots F^-$ using TD-B3LYP, TD-PBE0, TD-BLYP, and TD-OLYP. The corresponding values of λ_{abs} and λ_{fl} for BMP1 and $BMP1^-\cdots H^+\cdots F^-$ using other functionals are listed in Supplementary Table SIII. TD-B3LYP/6-31+G(d) method provides very good predictions for λ_{abs} of the BMP1 and deprotonated complex $BMP1^-\cdots H^+\cdots F^-$, as shown in Tables 2 and Supplementary SIII. The results are all in excellent agreement with experimental results [39], with the maximum deviation being less than 6 and 20 nm, respectively. However, the λ_{abs} value of anion form $BMP1^-$ at the same level is worsen accordance with the experimental data (deviation within 45 nm) than that for $BMP1^-\cdots H^+\cdots F^-$. The discrepancy may be ascribed to the neglecting of F^- in the stable complex $BMP1^-\cdots H^+\cdots F^-$. Thus, one may conclude that both the predicted λ_{abs} values for BMP1 and $BMP1^-\cdots H^+\cdots F^-$ are in good agreement with the experimental results (i.e., $\lambda_{abs} = 330$ and 425 nm before and after the addition of F^-). Using TD-B3LYP/6-31+G(d), the shift between the two characteristic λ_{abs} values for BMP1 and $BMP1^-\cdots H^+\cdots F^-$ is ca. 130 nm, which is comparable to the experimental 95 nm. The results displayed in Table 2 show that the TD-B3LYP calculations show poor performances for predicting the λ_{fl} for both BMP1 and $BMP1^-\cdots H^+\cdots F^-$. It is known that standard TD-DFT calculations show poor performances for charge-transfer electronic transitions [70, 71]. Other researchers [72, 73] have noted that the TD-B3LYP method does not correctly describe the delocalized excited states with charge-transfer component. The poor performance of the TD-B3LYP approach may be due to insufficient flexibility in the functional. More exhaustive investigations are needed before firm conclusions can be drawn, but from this study it appears that TD-B3LYP approaches may be limited in their usefulness for the studying of excited state relaxation for our system. Furthermore, the TD-OLYP/6-31+G(d) performs better in predicting the λ_{fl} for both BMP1 and $BMP1^-\cdots H^+\cdots F^-$ compared with the experimental data, with the maximum deviation being less than 14 nm. The shift between the two characteristic λ_{fl} values for BMP1 and $BMP1^-\cdots H^+\cdots F^-$ is ca. 156 nm, which is comparable to the experimental 158 nm. Thus, this result credits to the computational approach, so appropriate electronic transition energies can be predicted at these levels for such kind of chemosensor. The successful simulations indicate that the observed colorimetric and fluorescent signals truly originate from the formation of stable $BMP1^-\cdots H^+\cdots F^-$ complex. Furthermore, the λ_{abs} values of $BMP1^-$ using different functionals are worsen accordance with the experimental data than those for $BMP1\cdots H\cdots F^-$, indicating that the F^- has contribution to the molecular orbitals of $BMP1^-\cdots H^+\cdots F^-$.

The introduction of the solvent effects (PCM model) in the TD-DFT calculations leads to a slight bathochromic shifts for the λ_{abs} and λ_{fl} values of $BMP1^-\cdots H^+\cdots F^-$, which can be estimated to 10–12 nm compared with the values in gas phase. One can find that there is no drastic displacement of λ_{abs} and λ_{fl} for $BMP1^-\cdots H^+\cdots F^-$ when solvent effects are taken into account. However, the introduction of the solvent effects in the TD-DFT calculations leads to larger deviation of λ_{abs} and λ_{fl} for BMP1 from the experimental data. As PCM calculation is very time consuming for such large molecule, hereafter, we will not consider the solvent effects in the TD-DFT calculations.

Table 2 Calculated absorption λ_{abs} and fluorescence λ_{fl} wavelengths (in nm) of BMP1, $BMP1^-$, and $BMP1^-\cdots H^+\cdots F^-$ by various methods with 6-31+G(d) basis set, along with available experimental data

Methods	λ_{abs}			λ_{fl}		
	BMP1	$BMP1^-$	$BMP1^-\cdots H^+\cdots F^-$	BMP1	$BMP1^-$	$BMP1^-\cdots H^+\cdots F^-$
TD-B3LYP/6-31+G(d)	335.94 (361.40)[b]	470.08 (466.05)	405.56 (395.23)	380.12 (411.43)	512.09 (517.81)	487.02 (493.83)
TD-OLYP/6-31G+(d)	381.54 (414.92)	544.61 (540.93)	470.85 (458.20)	425.36 (462.51)	583.65 (590.94)	580.32 (568.27)
TD-PBE1PBE/6-31+G(d)	325.05 (347.94)	450.59 (445.56)	389.09 (379.15)	368.77 (397.41)	492.30 (496.19)	468.61 (473.98)
TD-BLYP/6-31+G(d)	386.54 (422.27)	553.74 (551.30)	545.64 (466.76)	430.71 (470.33)	593.73 (602.87)	582.88 (576.45)
Exp[a]	330		425	412		570

[a] Experimental data in MeCN solvent are from Ref. [39]

[b] Data in the parentheses are obtained considering PCM solvent effects

3.3 Electronic transition

The qualitative molecular orbital representations of the highest occupied molecular orbitals (HOMOs) and the lowest unoccupied molecular orbitals (LUMOs) for BMP1 and $BMP1^-\cdots H^+\cdots F^-$ in S_0 are shown in Fig. 1. In both cases, both the HOMOs and LUMOs have π characters. Each HOMO → LUMO transition corresponds to a π–π^* excited singlet state. The distribution patterns of HOMO and LUMO also provide a remarkable signature for the ICT transition. Analysis of the FMOs for BMP1 and $BMP1^-\cdots H^+\cdots F^-$ indicates that the excitation of the electron from the HOMO to the LUMO leads the electronic density to flow mainly from the benzoylamido and phenyl ring moieties to the imidine moiety in both BMP1 and $BMP1^-\cdots H^+\cdots F^-$. Inspection of Fig. 1 reveals clearly that the F^- definitely has some contribution to the HOMO, indicating that the most stable complex $BMP1^-\cdots H^+\cdots F^-$ is formed instead of isolated anion form $BMP1^-$ by the deprotonation process.

Comparing the geometry of BMP1 with $BMP1^-\cdots H^+\cdots F^-$, the bond lengths of C1–N7, N7–C8, C2–C3, C3–C17, C4–C19, and C5–C6 are shortened (see Table 3) after deprotonation, suggesting that the benzoylamido, phenyl ring, and imidine groups have strong conjugative effect. The molecular π-conjugation in $BMP1^-\cdots H^+\cdots F^-$ becomes higher than that of BMP1, because dihedral angles between phenyl and imidine groups become almost 0 or ±180°. As a consequence, the electron can flow easily from electron-donating benzoylamido and phenyl ring moieties to the electron-withdrawing imidine moiety. The photophysical properties of ICT are well known and highly dependent on the electron donor/acceptor strength [74–76]. It is obvious that deprotonation strengthens the electron-donating ability of benzoylamido group. Therefore, the ICT transition in the chemosensor system becomes much easier after deprotonation, resulting in the large bathochromic shift in their absorption and fluorescence spectra.

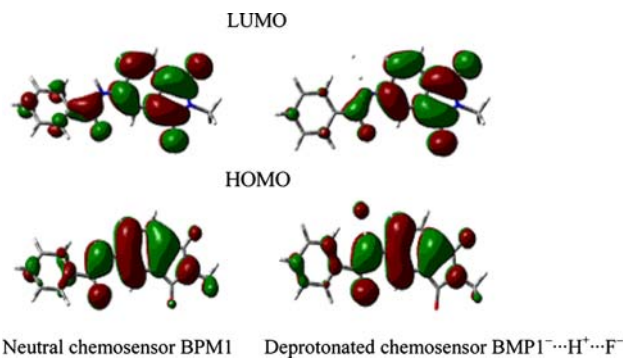

Fig. 1 FMOs for the neutral chemosensor BPM1 and deprotonated chemosensor $BMP1^-\cdots H^+\cdots F^-$ in the S_0 at the B3LYP/6-31+G(d) level

3.4 Substituent effect

3.4.1 Substituent effect on the electronic structures and properties of substituted derivatives

To study the substituent effect, we designed six BMP1 derivatives by introducing electron-donating [–$N(CH_3)_2$] or -withdrawing (–CN) group on either X or Y position or both (Scheme 1). The substituted derivatives BMP*n* ($n = 2$–7) were fully optimized without any symmetry constraints. The Cartesian coordinates of the substituted derivatives BMP*n* ($n = 2$–7) for the S_0 are given in Supplementary Table SIV. The introduction of the –$N(CH_3)_2$ and/or –CN groups for the parent compound leads to different changes of the electronic structures and properties. We compare the substituted derivatives with the parent compound in order to well understand the substituent effect.

Table 4 presents the calculated values of HOMO energy, LUMO energy, HOMO–LUMO gaps (E_g), absolute hardness (η), and absolute electronegativity (χ) for the BMP*n* ($n = 1$–7) at the B3LYP/6-31+G(d) level. Inspection of Table 4 reveals clearly that the –CN-substituted derivatives (BMP2 and BMP4) have the larger values of

Table 3 Main geometrical parameters (bond lengths in angstroms, angles and dihedral angles in degree) of BMP1 and BMP1$^-$···H$^+$···F$^-$ at the B3LYP/6-31+G(d) level

Bond parameter	Neutral chemosens BMP1	Deprotonated chemosensor BMP1$^-$···H$^+$···F$^-$
C1–N7	1.405	1.392
C1–C2	1.412	1.422
C1–C6	1.413	1.423
C2–C3	1.386	1.385
C3–C4	1.396	1.401
C3–C17	1.498	1.492
C4–C5	1.389	1.394
C4–C19	1.488	1.476
C5–C6	1.395	1.392
N7–C8	1.386	1.369
C8–C9	1.503	1.515
C8–O15	1.225	1.241
C9–C10	1.404	1.406
C17–O21	1.216	1.221
C17–N18	1.402	1.404
C19–O20	1.218	1.224
C19–N18	1.407	1.414
C1–N7–C8	129.0	125.8
N7–C8–C9	115.0	117.1
N7–C8–O15	123.1	123.9
C3–C2–C1–N7	179.2	180.0
C1–N7–C8–O15	2.94	0.01
C1–N7–C8–C9	−177.9	−180.0
N7–C8–C9–C10	28.0	−0.05

absolute hardness among the substituted derivatives investigated in this study. Hardness is the resistance of the chemical potential to change in the number of electrons, so that these special derivatives are expected to be more stable than other derivatives. The values of absolute hardness decrease when –N(CH$_3$)$_2$ or both –N(CH$_3$)$_2$ and –CN groups are introduced into BMP1, as listed in Table 4. The –N(CH$_3$)$_2$-substituted derivatives (BMP3 and BMP5) and bi-substituted derivatives (BMP6 and BMP7) have nearly equal values of absolute hardness, being clearly smaller than the value for BMP1, implying less stable than BMP1. The absolute electronegativity of the substituted derivatives increases when –CN group is introduced into BMP1, whereas the corresponding values decrease when –N(CH$_3$)$_2$ or both –N(CH$_3$)$_2$ and –CN groups are introduced into BMP1. The absolute electronegativity decreases in the sequence: BMP4 > BMP2 > BMP1 > BMP7 > BMP6 > BMP5 > BMP3. It also suggests that the –CN-substituted derivatives (BMP2 and BMP4) are expected to be more stable than BMP1 and other derivatives.

Table 4 Calculated values of HOMO energy, LUMO energy, HOMO–LUMO gaps E_g, absolute hardness η, and absolute electronegativity χ for the BMPn (n = 1–7) at the B3LYP/6-31+G(d) level (all in eV)

n	E_{LUMO}	E_{HOMO}	E_g	η	χ
1	−2.52	−6.81	4.29	2.15	4.67
2	−2.89	−7.10	4.21	2.10	5.00
3	−2.32	−5.88	3.56	1.78	4.10
4	−2.95	−7.27	4.32	2.16	5.11
5	−2.37	−6.05	3.68	1.84	4.21
6	−2.73	−6.04	3.31	1.66	4.39
7	−2.78	−6.24	3.47	1.73	4.51

3.4.2 *Substituent effect on the BSSE-corrected interaction energy (ΔE_{BSSE}) of deprotonated derivatives complexes*

Table 5 presents the ΔE_{BSSE} of complexes BMPn^-···H$^+$···F$^-$, BMPn·Cl$^-$, and BMPn·Br$^-$ (n = 1–7). As the counterpoise correction was unreliable for H-bond with fluorine in some cases [77], we also calculated the ΔE of complexes BMPn^-···H$^+$···F$^-$, BMPn·Cl$^-$, and BMPn·Br$^-$ (the data in parentheses in Table 5) without BSSE correction and compared with the ΔE_{BSSE}. The MeCN solvent effect also has been considered using the different models such as PCM, CPCM, IEF-PCM, COSMORS, and Onsager models [78]. The ΔE values of both BMPn^-···H$^+$···F$^-$ and BMPn·Br$^-$ are only about −3 approximately to −5 kcal/mol, whereas the corresponding values of BMPn·Cl$^-$ are positive (∼4 kcal/mol) using PCM, CPCM, IEF-PCM, and COSMORS models, suggesting the impropriety for PCM in the strong polarity for MeCN [79, 80]. However, the Onsager model provides acceptable ΔE values compared with other solvent models. The ΔE values considering solvent effect ($\Delta E_{Onsager}$) are given in Supplementary Table SV. The Cartesian coordinates of the substituted derivative complexes BMPn^-···H$^+$···F$^-$ (n = 2–7) with the BSSE correction for

Table 5 ΔE_{BSSE} (in kcal/mol) of complexes BMPn^-···H$^+$···F$^-$, BMPn·Cl$^-$, and BMPn·Br$^-$ (n = 1–7) at the B3LYP/6-31+G(d) level

n	BMPn^-···H$^+$···F$^-$	BMPn·Cl$^-$	BMPn·Br$^-$
1	−55.16 (−57.02)[a]	−31.83 (−32.14)	−27.71 (−35.60)
2	−62.87 (−64.71)	−38.15 (−38.36)	−33.69 (−41.70)
3	−51.80 (−53.65)	−29.22 (−29.51)	−25.29 (−33.01)
4	−59.86 (−62.49)	−35.19 (−35.50)	−30.59 (−38.73)
5	−54.72 (−56.62)	−32.21 (−32.53)	−28.12 (−36.00)
6	−56.94 (−58.86)	−32.32 (−32.64)	−27.89 (−34.45)
7	−62.23 (−64.12)	−38.36 (−38.66)	−33.90 (−40.77)

[a] Data in the parentheses are obtained without considering BSSE corrections

the S_0 are given in Supplementary Table SVI. The ΔE_{BSSE} of the deprotonated –CN-substituted derivative complexes ($BMP2^-\cdots H^+\cdots F^-$ and $BMP4^-\cdots H^+\cdots F^-$) are more negative by 7.71 and 4.70 kcal/mol than that of $BMP1^-\cdots H^+\cdots F^-$, respectively, as shown in Table 5. To the contrary, the corresponding values of the deprotonated $-N(CH_3)_2$-substituted derivative complexes ($BMP3^-\cdots H^+\cdots F^-$ and $BMP5^-\cdots H^+\cdots F^-$) are more positive by 3.36 and 0.44 kcal/mol than that of $BMP1^-\cdots H^+\cdots F^-$, respectively. The ΔE_{BSSE} of the deprotonated bi-substituted derivative complexes ($BMP6^-\cdots H^+\cdots F^-$ and $BMP7^-\cdots H^+\cdots F^-$) are more negative by 1.78 and 7.07 kcal/mol than that of $BMP1^-\cdots H^+\cdots F^-$, respectively. This indicates that the ΔE_{BSSE} values of the deprotonated derivatives depend mostly on the –CN group and its position, whereas it is not in the same case for BMP*n*·Cl^- and BMP*n*·Br^- (only in the range of 30–40 kcal/mol). Furthermore, the ΔE values of all complexes $BMPn^-\cdots H^+\cdots F^-$, BMP*n*·$Cl^-$, and BMP*n*·$Br^-$ ($n = 1$–7) are similar to those of ΔE_{BSSE} (the maximum difference being less than 8 kcal/mol), indicating that the counterpoise correction is in a reasonable range. Furthermore, the solvent effect does not significantly affect the $\Delta E_{Onsager}$ compared with those ΔE without considering solvent effect (see Tables 5 and Supplementary Table SV).

3.4.3 *Substituent effect on the absorption spectra of the derivatives and their deprotonated complexes*

Table 6 presents the assignment, excitation energies, λ_{abs}, and the oscillator strength (*f*). The absorption can be mainly assigned to the HOMO → LUMO. The λ_{abs} of the $-N(CH_3)_2$-substituted derivatives (BMP3 and BMP5) has bathochromic shifts (50 and 66 nm) compared with the parent compound BMP1, whereas the corresponding values of the –CN-substituted derivatives (BMP2 and BMP4) are similar to that of BMP1, with the deviation <5 nm. The λ_{abs} of bi-substituted derivatives (BMP6 and BMP7) has strong bathochromic shifts (80 and 82 nm). In general, larger oscillator strength corresponds to larger experimental absorption coefficient or stronger fluorescence intensity. The *f* value of the –CN-substituted derivative BMP2 is the greatest among the derivatives, corresponding to the most intensive spectrum. It suggests that the $-N(CH_3)_2$ substitution has more influence on the shifts of λ_{abs} for the substituted derivatives, whereas the –CN substitution does not significantly affect the absorption spectra. For the deprotonated-substituted derivative complexes, it is found that all the λ_{abs} are similar to that of the parent complex $BMP1^-\cdots H^+\cdots F^-$ (deviation within 25 nm). They show greater *f* values than that of the parent complex $BMP1^-\cdots H^+\cdots F^-$ except that the *f* values of $BMP5^-\cdots H^+\cdots F^-$ and $BMP7^-\cdots H^+\cdots F^-$ are less than that of the parent complex $BMP1^-\cdots H^+\cdots F^-$. Therefore the $-N(CH_3)_2$ and –CN substitutions do not significantly affect the absorption spectra of the deprotonated-substituted derivative complexes. It clearly shows that the –CN-substituted derivatives (BMP2 and BMP4) and their deprotonated complexes have more intense absorption spectra than that of BMP1.

On the basis of the results described above, one can conclude that all the substituted derivatives BMP*n* ($n = 2$–7) are expected to be chromogenic chemosensors. The colorless solutions of BMP*n* ($n = 2$–4) turn yellow in the present F^- as parent compound BMP1, whereas olivine solution of BMP*n* ($n = 5$–7) turns yellow upon addition of F^-.

3.4.4 *Substituent effect on the fluorescence spectra of the derivatives and their deprotonated complexes*

The Cartesian coordinates of the substituted derivatives BMP*n* and their complexes $BMPn^-\cdots H^+\cdots F^-$ ($n = 2$–7) for the S_1 are given in Supplementary Tables SVII and

Table 6 Calculated maximum absorption wavelengths λ_{abs} (in nm), oscillator strength *f*, and excitation energies *E* (in eV) of BMP*n* and $BMPn^-\cdots H^+\cdots F^-$ ($n = 1$–7) at the TD-B3LYP/6-31+G(d) level

n	BMP*n*				$BMPn^-\cdots H^+\cdots F^-$			
	Assignment	*E*	λ_{abs}	*f*	Assignment	*E*	λ_{abs}	*f*
1	H → L (0.65)	3.69	335.94	0.16	H → L (0.65)	3.06	405.56	0.19
2	H → L (0.64)	3.69	336.45	0.27	H → L (0.65)	3.11	398.64	0.27
3	H → L (0.69)	3.21	385.86	0.18	H → L (0.65)	2.95	419.73	0.26
4	H → L (0.64)	3.74	331.64	0.18	H → L (0.64)	2.93	422.69	0.26
5	H → L (0.66)	3.09	400.81	0.10	H → L (0.64)	3.03	409.82	0.14
6	H → L (0.70)	2.98	415.88	0.16	H → L (0.67)	2.88	430.33	0.28
7	H → L (0.66)	2.97	417.18	0.09	H → L (0.65)	3.18	417.01	0.12
Exp[a]			330				425	

[a] Experimental data in MeCN solvent are from Ref. [39]

Table 7 Calculated maximum fluorescence wavelengths λ_{fl} (in nm), oscillator strength f, excitation energies E (in eV), and radiative rate constant k_f (in 10^7 S^{-1}) of BMPn and BMP$n^-\cdots H^+\cdots F^-$ (n = 1–7) at the TD-OLYP/6-31+G(d) level

n	BMPn					BMP1$^-\cdots$H$^+\cdots$F$^-$				
	Assignment	E	λ_{fl}	f	k_f	Assignment	E	λ_{fl}	f	k_f
1	H ← L (0.64)	2.91	425.36	0.11	4.05	H ← L (0.44)	2.14	580.32	0.04	0.79
						H-1 ← L (0.52)				
2	H ← L (0.62)	2.86	431.51	0.20	7.16	H ← L (0.67)	1.55	798.27	0.06	0.63
	H ← L + 1 (−0.18)									
3	H ← L (0.68)	2.19	565.43	0.08	1.67	H-2 ← L (0.40)	2.21	560.40	0.12	2.55
	H-1 ← L (−0.14)					H-1 ← L (−0.36)				
4	H ← L (0.64)	2.99	415.11	0.12	4.64	H ← L (0.49)	2.38	521.56	0.15	3.68
	H-3 ← L (0.12)					H ← L + 1 (0.39)				
5	H ← L (0.63)	2.48	500.44	0.08	2.13	H ← L (0.28)	2.53	490.64	0.13	3.60
						H-4 ← L (0.50)				
6	H ← L (0.69)	2.00	618.45	0.09	1.57	H ← L (0.49)	2.10	591.76	0.12	2.28
						H-4 ← L (0.33)				
7	H ← L (0.61)	2.17	572.42	0.04	0.81	H ← L (0.42)	2.14	578.31	0.02	0.40
	H ← L + 1 (−0.32)					H-2 ← L (0.44)				
Exp[a]			412					570		

[a] Experimental data in MeCN solvent are from Ref. [39]

SVIII, respectively. Table 7 presents the assignment, excitation energies, λ_{fl}, the oscillator strength (f), and the radiative rate constant (k_f). The λ_{fl} of the –N(CH$_3$)$_2$-substituted derivatives (BMP3 and BMP5) have bathochromic shifts (140 and 75 nm) compared with the BMP1. The corresponding values of the –CN-substituted derivatives (BMP2 and BMP4) are similar to that of BMP1, with the deviations being less than 11 nm. The λ_{fl} values of the bi-substituted derivatives (BMP6 and BMP7) show strong bathochromic shifts (193 and 147 nm) compared with BMP1. Furthermore, the f values of the –CN-substituted derivatives (BMP2 and BMP4) are greater than the rest, corresponding to stronger fluorescence spectra. It suggests that the –N(CH$_3$)$_2$ substitution shows more influence on the shifts of λ_{fl} in the derivatives. For the deprotonated-substituted complexes, one can find that λ_{fl} of the deprotonated-substituted complex with –CN on the benzoylamido moiety (BMP2$^-\cdots$H$^+\cdots$F$^-$) shows hypsochromic shift (218 nm), whereas with –N(CH$_3$)$_2$ on the benzoylamido moiety (BMP3$^-\cdots$H$^+\cdots$F$^-$) shows bathochromic shift (20 nm) compared with BMP1$^-\cdots$H$^+\cdots$F$^-$. The λ_{fl} of the deprotonated-substituted complexes with a group on the methylphthalimide moiety (BMP4$^-\cdots$H$^+\cdots$F$^-$ and BMP5$^-\cdots$H$^+\cdots$F$^-$) show hypsochromic shifts (68 and 90 nm). The λ_{fl} of the deprotonated bi-substituted derivative complexes (BMP6$^-\cdots$H$^+\cdots$F$^-$ and BMP7$^-\cdots$H$^+\cdots$F$^-$) are similar to that of the BMP1$^-\cdots$H$^+\cdots$F$^-$ (deviations within 11 nm). Hence, either –N(CH$_3$)$_2$ or –CN group on the methylphthalimide moiety can affect significantly the fluorescence spectra of the deprotonated derivative complexes. Furthermore, the substituted derivative complexes with a substituent on the methylphthalimide moiety (BMP4$^-\cdots$H$^+\cdots$F$^-$ and BMP5$^-\cdots$H$^+\cdots$F$^-$) show greater f values for the λ_{fl} than those of BMP1$^-\cdots$H$^+\cdots$F$^-$ and other substituted derivatives, implying that the substituted position plays a key role in enhancing f value. Thus, one may conclude that the fluorescence intensity can be increased by the introduction of the groups on the methylphthalimide moiety of BMP1.

One can find that the –CN-substituted derivatives (BMP2 and BMP4) show greater k_f values than those of BMP1 and other derivatives, as shown in Table 7. It indicates that the –CN-substituted derivatives have higher fluorescence quantum yields than those of the –N(CH$_3$)$_2$-substituted derivatives (BMP3 and BMP5) and bi-substituted derivatives (BMP6 and BMP7). For the deprotonated derivative complexes, the k_f values of the derivative complexes with a group on the methylphthalimide moiety (BMP4$^-\cdots$H$^+\cdots$F$^-$ and BMP5$^-\cdots$H$^+\cdots$F$^-$) are greater than the rest. Hence, the derivatives with a substituent on the methylphthalimide moiety have higher fluorescence quantum yields than other derivatives when the concentration of F$^-$ anions reaches certain level from the addition of tetrabutylammonium fluoride to the sensor substrate solution.

The bathochromic shift between the two characteristic λ_{fl} values (i.e., λ_{fl} values before and after the addition of F$^-$) for BMP2 and its deprotonated complex is 367 nm. This implies that the intensity of the blue-purple original fluorescence for BMP2 decreased and its color changes from blue-purple to colorless. For BMP3 and BMP7, the

shifts between the two characteristic λ_{fl} values are only 5–6 nm. Thus, they have not distinct fluorescence color change upon the addition of F^-, implying that the derivatives BMP3 and BMP7 are not suitable to be ratiometric fluorescent fluoride chemosensor as BMP2. The bathochromic shift between the two characteristic λ_{fl} values for BMP4 and its deprotonated complex is 106 nm. It indicates that the intensity of the purple original fluorescence for BMP4 decreased, along with the appearance of a new green emission upon the addition of F^-. The hypsochromic shifts between the two characteristic λ_{fl} values for BMP5 and BMP6 and their deprotonated complexes are 10 and 27 nm, respectively. Therefore, a decrease in turquoise and orange original fluorescence intensity of BMP5 and BMP6 may be observed and new blue and yellow emissions appear upon the addition of F^-, respectively.

Our results suggest that the mono-substituted (on the methylphthalimide moiety) and bi-substituted [–$N(CH_3)_2$ and –CN groups on benzoylamido and methylphthalimide moieties, respectively] derivatives are expected to be promising candidates for ratiometric fluorescent fluoride chemosensors. Furthermore, the mono–CN-substituted derivatives are promising luminescent materials for OLEDs as well.

4 Conclusions

Our calculated results for both the host–guest interaction and the nature of colorimetric and fluorescent signaling for BMP1 in the presence of fluoride anion are in good agreement with the reported experimental observations. The host chemosensor BMP1 has much stronger affinity to F^- than to Cl^- or Br^-, which provides a way for the proton transfer back and forth between the sensor substrate and F^-. The FMO analysis has turned out that the vertical electronic transitions of absorption and emission in both BMP1 and $BMP1^-\cdots H^+\cdots F^-$ correspond to the sensing signals due to the ICT. The fluorine atom has contributed to the HOMO of $BMP1^-\cdots H^+\cdots F^-$, indicating that the F^- affects the HOMO–LUMO gap of $BMP1^-\cdots H^+\cdots F^-$. The deprotonated complex $BMP1^-\cdots H^+\cdots F^-$ is formed instead of isolated anion form $BMP1^-$ by the deprotonation process of chemosensor. The inclusion of diffuse functions to the basis set has a significant effect on the simulation results. The study of substituent effect by introducing electron-donating [–$N(CH_3)_2$] or -withdrawing (–CN) group on either benzoylamido or methylphthalimide moiety or both revealed that the –CN substitutions increase stabilities of the substituted derivatives, whereas –$N(CH_3)_2$ substitutions decrease the stabilities of the substituted derivatives compared with the parent compound BMP1. Both λ_{abs} and λ_{fl} of the mono–$N(CH_3)_2$ substituted derivatives show a strong bathochromic shift compared with BMP1, whereas the corresponding values of the mono–CN substituted derivatives are similar to that of BMP1. For the deprotonated derivative complexes, their λ_{abs} values are similar to that of the parent complex $BMP1^-\cdots H^+\cdots F^-$, while the substituent on methylphthalimide moiety can effectively tune the λ_{fl} of the designed complexes. The –CN substituent results in the derivatives and their deprotonated complexes possessing more intense absorption and fluorescence spectra than BMP1 and other derivatives. Our results suggest that the mono-substituted (on the methylphthalimide moiety) and bi-substituted [–$N(CH_3)_2$ and –CN groups on benzoylamido and methylphthalimide moieties, respectively] derivatives are expected to be promising candidates for ratiometric fluorescent fluoride chemosensors as well as chromogenic chemosensor, whereas for mono-substituted (on the benzoylamido moiety) and bi-substituted [–CN and –$N(CH_3)_2$ on benzoylamido and methylphthalimide moieties, respectively] derivative can serve as chromogenic fluoride chemosensor. Furthermore, the derivatives with mono–CN substituents are promising luminescent materials for OLEDs as well.

Acknowledgments Financial supports from the NSFC (Nos. 50873020 and 20773022), the NCET-06-0321, the JLSDP (20082212), and the NENU-STB-07-007 are gratefully acknowledged.

References

1. Gassensmith JJ, Arunkumar E, Barr L, Baumes JM, DiVittorio KM, Johnson JR, Noll BC, Smith BD (2007) J Am Chem Soc 129:15054
2. Anai T, Nakata E, Koshi Y, Ojida A, Hamachi I (2007) J Am Chem Soc 129:6232
3. Palacios MA, Nishiyabu R, Marquez M, Anzenbacher P Jr (2007) J Am Chem Soc 129:7538
4. Hagihara S, Tanaka H, Matile S (2008) J Am Chem Soc 130:5656
5. Li JQ, Li XY (2007) J Phys Chem A 111:13061
6. Yoon J, Kim SK, Singh NJ, Kim KS (2006) Chem Soc Rev 35:355
7. Gale PA (2006) Acc Chem Res 39:465
8. Beer PD, Gale PA (2001) Angew Chem Int Ed Engl 40:486
9. Callan JF, de Silva AP, Magri DC (2005) Tetrahedron 61:8551
10. Czarnik AW (1994) Acc Chem Res 27:302
11. Fabbrizzi L, Poggi A (1995) Chem Soc Rev 24:197
12. Martinez-Manez R, Sancanon F (2003) Chem Rev 103:4419
13. Mondal CK, Lee JY (2006) J Theor Comput Chem 5:857
14. Sarkar M, Samanta A (2008) J Mol Struct Theochem 863:111
15. Valeur B (2002) Molecular fluorescence. Wiley-VCH, Weinhein, Germany
16. Kirk KL (1991) Biochemistry of the halogens and inorganic halides. Plenum Press, New York, p 58
17. Lee JY, Cho EJ, Mukamel S, Nam KC (2004) J Org Chem 69:943
18. Kleerekoper M (1998) Endocrinol Metab Clin North Am 27:441
19. Briancon D (1997) Revue du Rhumatisme 64:78 (English edition)

20. Kissa E (1987) Clin Chem 33:253
21. Sohn H, Létant S, Sailor MJ, Trogler WC (2000) J Am Chem Soc 122:5399
22. Zhang SW, Swager TM (2003) J Am Chem Soc 125:3420
23. Kim SK, Yoon J (2002) Chem Commun 770
24. Ghosh K, Masanta G (2006) Tetrahedron Lett 47:2365
25. Thiagarajan V, Ramamurthy P (2007) Spectrochim Acta A 67:772
26. Thiagarajan V, Indirapriyadharshini VK, Ramamurthy P (2006) J Incl Phenom Macro 56:309
27. Choi K, Hamilton AD (2001) Angew Chem Int Ed Engl 40:3912
28. Peng X, Wu Y, Fan J, Tian M, Han K (2005) J Org Chem 70:10524
29. Zhang X, Guo L, Wu FY, Jiang YB (2003) Org Lett 5:2667
30. Tong H, Zhou G, Wang L, Jing X, Wang F, Zhang J (2003) Tetrahedron Lett 44:131
31. Thiagarajan V, Ramamurthy P, Thirumalai D, Ramakrishnan VT (2005) Org Lett 7:657
32. Li Z, Zhang J (2006) Chem Phys 331:159
33. Thiagarajan V, Ramamurthy P (2007) J Lumin 126:886
34. Kim SK, Bok JH, Bartsch RA, Lee JY, Kim JS (2005) Org Lett 7:4839
35. Nishizawa S, Kato Y, Teramae N (1999) J Am Chem Soc 121:9463
36. Wu JS, Zhou JH, Wang PF, Zhang XD, Wu SK (2005) Org Lett 7:2133
37. Beer PD (1998) Acc Chem Res 31:71
38. Chow CF, Chiu BKW, Lam MHW, Wong WY (2003) J Am Chem Soc 125:7802
39. Sarkar M, Yellampalli R, Bhattacharya B, Kanaparthi RK, Samanta A (2007) J Chem Sci 119:91
40. Boys SF, Bernardi F (1970) Mol Phys 19:553
41. Simon S, Duran M, Dannenberg JJ (1996) J Chem Phys 105:11024
42. Muhammad S, Liu C, Zhao L, Wu S, Su Z (2009) Theor Chem Acc 122:77
43. Hlawacek G, Puschnig P, Frank P, Winkler A, Ambrosch-Drax C, Teichert C (2008) Science 321:108
44. Rogach AL, Gaponik N, Lupton JM, Bertoni C, Gallardo DE, Dunn S, Li Pira N, Paderi M, Repetto P, Romanov SG, O'Dwyer C, Sotomayor Torres CM, Eychmüller A (2008) Angew Chem Int Ed Engl 47:6538
45. Lo SC, Bera RN, Harding RE, Burn PL, Samuel IDW (2008) Adv Funct Mater 18:3080
46. Haldi A, Kimyonok A, Domercq B, Hayden LE, Jones SC, Marder SR, Weck M, Kippelen B (2008) Adv Funct Mater 18:3056
47. Ding J, Lü J, Cheng Y, Xie Z, Wang L, Jing X, Wang F (2008) Adv Funct Mater 18:2754
48. Ning Z, Chen Z, Zhang Q, Yan Y, Qian S, Cao Y, Tian H (2007) Adv Funct Mater 17:3799
49. Ki W, Li J (2008) J Am Chem Soc 130:8114
50. Montes VA, Perez-Bolıvar C, Estrada LA, Shinar J, Anzenbacher P Jr (2007) J Am Chem Soc 129:12598
51. Yang R, Wu H, Cao Y, Bazan GC (2006) J Am Chem Soc 128:14422
52. Ni J, Yan H, Wang A, Yang Y, Stern CL, Metz AW, Jin S, Wang L, Marks TJ, Ireland JR, Kannewurf CR (2005) J Am Chem Soc 127:5613
53. Frisch MJ, Trucks GW, Schlegel HB, Scuseria GE, Robb MA, Cheeseman JR, Montgomery JAJ, Vreven T, Kudin KN, Burant JC, Millam JM, Iyengar SS, Tomasi J, Barone V, Mennucci B, Cossi M, Scalmani G, Rega N, Petersson GA, Nakatsuji H, Hada M, Ehara M, Toyota K, Fukuda R, Hasegawa J, Ishida M, Nakajima T, Honda Y, Kitao O, Nakai H, Klene M, Li X, Knox JE, Hratchian HP, Cross JB, Adamo C, Jaramillo J, Gomperts R, Stratmann RE, Yazyev O, Austin AJ, Cammi R, Pomelli C, Ochterski JW, Ayala PY, Morokuma K, Voth GA, Salvador P, Dannenberg JJ, Zakrzewski VG, Dapprich S, Daniels AD, Strain MC, Farkas O, Malick DK, Rabuck AD, Raghavachari K, Foresman JB, Ortiz JV, Cui Q, Baboul AG, Clifford S, Cioslowski J, Stefanov BB, Liu G, Liashenko A, Piskorz P, Komaromi I, Martin RL, Fox DJ, Keith T, Al-Laham MA, Peng CY, Nanayakkara A, Challacombe M, Gill PMW, Johnson B, Chen W, Wong MW, Gonzalez C, Pople JA (2004) Gaussian 03, revision C.02. Gaussian Inc., Wallingford, CT
54. Becke AD (1993) J Chem Phys 98:5648
55. Foresman JB, Head-Gordon M, Pople JA, Frisch MJ (1992) J Phys Chem 96:135
56. Sun M, Niu B, Zhang J (2008) J Mol Struct Theochem 862:85
57. Gahungu G, Zhang J (2005) J Mol Struct Theochem 755:19
58. Cossi M, Rega N, Scalmani G, Barone V (2003) J Comput Chem 24:669
59. Ahlrichs R, Bar M, Haser M, Horn H, Kolmel C (1989) Chem Phys Lett 162:16
60. Parr RG, Yang W (1989) Density-functional theory of atoms and molecules. Oxford Science Publications, Oxford University Press, New York
61. Parr RG, Pearson RG (1983) J Am Chem Soc 105:7512
62. Pearson RG (1985) J Am Chem Soc 107:6801
63. Start MS (1997) J Phys Chem A 101:8296
64. Koopmans T (1934) Physica 1:104
65. Doroshenko AO, Posokhov EA, Verezubova AA, Ptyagina LM (2000) J Phys Org Chem 13:253
66. Aquino AJA, Lischka H, Hattig C (2005) J Phys Chem A 109:3201
67. Joachain CJ, Brandsen BH (1983) Physics of atoms and molecules. Longman Group Limited, London
68. Steiner T, Desiraju GR (1998) Chem Commun 891
69. Steiner T (2002) Angew Chem Int Ed Engl 41:48
70. Dreuw A, Fleming GR, Head-Gordon M (2003) J Phys Chem B 107:6500
71. Dreuw A, Head-Gordon M (2004) J Am Chem Soc 126:4007
72. Walker RC, Mercer IP, Gould IR, Klug DR (2006) J Comput Chem 28:478
73. Tozer DJ, Amos RD, Handy NC, Roos BO, Serrano-Andres L (1999) Mol Phys 97:859
74. Liu B, Tian H (2005) J Mater Chem 15:2681
75. Wen Z, Jiang Y (2004) Tetrahedron 60:11109
76. Huang W, Zhang X, Ma L, Wang C, Jiang Y (2002) Chem Phys Lett 352:401
77. Schwenke DW, Truhlar DG (1985) J Chem Phys 82:2418
78. Wong MW, Wiberg KB, Frisch MJ (1992) J Am Chem Soc 114:1645
79. Cramer CJ, Truhlar DG (2009) Acc Chem Res 42:493
80. Meng S, Ma J (2008) J Phys Chem B 112:4313